

This is the preprint version of our accepted manuscript published on 22 June 2023 in *Nanoscale* :
<https://doi.org/10.1039/D3NR02378H>

Ultra-stable Silver Nanoplates: Efficient and Versatile Colorimetric Reporters for Dipstick Assays

Received 00th January 20xx,
 Accepted 00th January 20xx

Maurice Retout,^{a,#} Bryan Gosselin,^{a,b,#} Amina Adrovic,^{a,b} Pascale Blond,^b Ivan Jabin,^{b,*} and Gilles Bruylants,^{a,*}

DOI: 10.1039/x0xx00000x

Abstract

Noble metal anisotropic nanostructures, such as silver nanoplates (AgNPLs), are interesting because they possess enhanced plasmonic properties compared to their spherical counterparts: increased extinction coefficient and tunable maximum of absorption wavelength. However, their use for biosensing application is limited as these structures are intrinsically unstable and, to maintain the anisotropic structure, a coating protecting the metallic surface is required. In this work, we report on the capacity of a thin but robust coating based on calixarene-diazonium salts to maintain the structure anisotropy of silver nanoplates in conditions in which traditionally used coatings fail. We synthesized AgNPLs of various sizes and coated them with two different calixarenes, differing by the functional groups attached to their small rim. After characterization of the efficiency of the ligand exchange process between the initial citrate anions and the calixarenes, the chemical and colloidal stabilities of the resulting calixarene-coated AgNPLs were compared to citrate-capped AgNPLs. A radical improvement of the lifetime of the material from 1 day for AgNPLs coated with citrate to more than 900 days for calixarene-coated AgNPLs, as well as the stability in acidic conditions, phosphate saline buffer (PBS) or biofluid, were

observed. Benefiting from this exceptional robustness, calixarene-coated AgNPLs were exploited to design dipstick assays. Rabbit immunoglobulin G (IgG) detection was developed first as proof-of-concept. The optimal system was then used for the detection of Anti-SARS-CoV-2 IgG. In both cases, a picomolar limit of detection (LOD) was achieved as well as the detection in 100% of pooled human plasma. This sensitivity competes with that of ELISA and is better than the one previously obtained with gold or even silver nanospheres for the same target and in similar conditions. Finally, the wide range of colors provided by the AgNPLs allowed the design of a multicolor multiplex assay for the simultaneous detection of multiple analytes.

Introduction

The last decade has witnessed an increase of interest for the use of nanomaterials in biomedical applications.^{1,2} In particular, plasmonic nanomaterials have been the subject of extensive research as their Localized Surface Plasmon Resonance (LSPR) band can be finely modulated according to their size, shape or metal composition,^{3,4} making them adequate colorimetric reporters for biosensing devices.^{5,6} Due to their ease of manipulation, spherical gold nanoparticles (AuNPs)⁷ have been massively used in this context,^{8–10} and notably for the detection of viruses,¹¹ proteins^{12,13} or nucleic acids.¹⁴ Silver nanoparticles (AgNPs) have an extinction coefficient that is approximately one order of magnitude higher than AuNPs of similar size.¹⁵ However, these nanomaterials are much less exploited as colorimetric reporters because they

^a Engineering of Molecular NanoSystems, Ecole Polytechnique de Bruxelles, Université libre de Bruxelles (ULB), avenue F. D. Roosevelt 50, CP165/64, B-1050 Brussels, Belgium.

^b Address here. Laboratoire de Chimie Organique, Université libre de Bruxelles (ULB), avenue F. D. Roosevelt 50, CP160/06, B-1050 Brussels, Belgium.

[#] Authors contributed equally.

* Corresponding authors.

Electronic Supplementary Information (ESI) available: [Materials, Instrumentation, Characterization of AgNPLs^{DF-C2}, Stability study of various sizes of AgNPLs^{DF-C1}, Bioconjugation of various sizes of AgNPLs^{DF-C1}, Dipstick assay for the detection of Rabbit IgG with various sizes of AgNPLs^{DF-C1}]. See DOI: 10.1039/x0xx00000x

are highly sensitive to oxidative conditions.¹⁶ Their conjugation to biomolecules is therefore limited and typically requires a first protective coating of the metallic core.^{17,18}

In this context, we have recently reported the synthesis of ultra-stable Ag or AuNPs¹⁹ and their use as colorimetric reporter in biosensing applications.^{20–22} For this, the nanoparticles were stabilized with an ultra-thin calixarene-based layer obtained from the reductive grafting of calixarene-tetradiazonium salts.^{23,24} Up to four bonds per calixarene can be formed with the surface, leading to a strongly anchored organic layer that provides extreme resistance to the nanomaterial and enables its conjugation with biomolecules. Calixarene-coated Ag or AuNPs have demonstrated a superior stability compared to particles with traditional coatings, allowing their drying and resuspension or their use in biofluids.^{21,25–27} Very recently, we have shown that calixarene-coated AgNPs could advantageously replace gold nanoparticles of the same size (i.e. around 20 nm) in a serological dipstick assay for the detection of Anti-SARS-CoV-2 Immunoglobulin G.²² An improvement by one order of magnitude of the limit of detection was indeed obtained compared to AuNPs due to the better optical properties of silver. However, due to a lack of contrast with the white strip, the yellow band generated at the test line by the 20 nm AgNPs was difficult to observe with the naked eye. To overcome this limitation, we envisioned the use of silver nanoplates (AgNPLs) as colorimetric reporters. Indeed, AgNPLs are a promising class of silver-based nanomaterials,²⁸ which, compared to spherical particles, display enhanced optical properties that can be easily tuned via structural changes such as edge sharpness or aspect ratio.^{29–31} While AgNPLs are classically used for SERS applications,³² they could also be exploited for colorimetric assays as i) they can offer a multitude of colors³³ and ii) a lower amount of material could be used per test thanks to their higher extinction coefficient than corresponding spherical particles. However, the use of AgNPLs in biosensing applications is even more limited than that of AgNPs, due to their even lower

stability. Upon exposure to light, heat, oxidative conditions or various chemicals, the triangular shape evolves through etching towards disks structures that possess a lower surface energy,^{34–36} making the functionalization of AgNPLs with recognition elements extremely difficult.^{37,38} Therefore, only few examples of dipstick or lateral-flow assays involving AgNPLs are reported in the literature.^{39,40}

Herein, we report on the stabilization of AgNPLs with a thin and bioconjugable calixarene-based layer. We synthesized citrate-capped AgNPLs of various sizes and exchanged the citrate anions with two different calixarenes differing by the functional groups at the level of their small rim. The improvement of the colloidal and chemical stabilities of the resulting AgNPLs was evaluated as well as their capacity to be suspended in biofluids. A calixarene-coated AgNPLs based dipstick assay for the detection of Rabbit IgG was then developed as a proof-of-concept. Finally, the system was applied to the serological sensing of Anti-SARS-CoV-2 IgG and, ultimately, to a combination of these two targets in a multicolor multiplex assay.

Results and discussion

Synthesis of calixarene-coated AgNPLs. Two calixarene-tetradiazonium salts differing by their functionalities at the level of their small rim were used to stabilize the AgNPLs: one bearing four carboxyl groups (**C1**) and one bearing four Poly(Ethylene Glycol) (PEG) chains ended by methoxy groups (**C2**) (inset **Figure 1**). These calixarenes were selected as it was shown that they confer distinct properties to the surfaces on which they are grafted.¹⁹ On the one hand, the carboxyl groups of **C1** ensure the colloidal stability of particles at pH > 6 and can serve to the covalent conjugation of biomolecules through the formation of amide bonds.^{19,26} On the other hand, the grafting of **C2** leads to a dense PEG layer that enables a steric stabilization of the particles.²⁶

The synthesis of the AgNPLs was inspired from a seed-growth procedure reported previously

by Haber *et al.*³³ Briefly, silver seeds were produced in deionized water via the reduction of silver nitrate (AgNO_3) by sodium borohydride (NaBH_4) in the presence of trisodium citrate and hydrogen peroxide (H_2O_2) (**Figure 1**). The seeds were then grown into AgNPs via i) dropwise addition of AgNO_3 in presence of ascorbic acid, ii) dilution by a factor two and iii) again dropwise addition of AgNO_3 after addition of ascorbic acid (1st growth). The color of the suspension turned from yellow to red-pink as AgNPs were produced. This suspension of AgNPs, named $\text{AgNPs}^0\text{-citrate}$, was used to generate larger AgNPs via a last cycle of dilution (either with a factor of 4, 8, 20, 40 or 80) and dropwise addition of AgNO_3 and ascorbic acid (2nd growth). The color of the different batches of AgNPs, named $\text{AgNPs}^{\text{Df-citrate}}$ with Df represents the dilution factor from $\text{AgNPs}^0\text{-citrate}$, was related to Df (see below). The citrate ligands at the surface of the NPs were then replaced by calix[4]arenes through a ligand exchange process. For this, a solution of calix[4]arene-tetradiazonium salt **C1** or **C2** and NaBH_4 was added to all batches of AgNPs, from $\text{AgNPs}^0\text{-citrate}$ to $\text{AgNPs}^{\text{Df-citrate}}$, and the suspensions were stirred overnight, leading to either $\text{AgNPs}^{\text{Df-C1}}$, $\text{AgNPs}^{\text{Df-C1}}$, $\text{AgNPs}^{\text{Df-C2}}$ or

$\text{AgNPs}^{\text{Df-C2}}$. It is noteworthy that NaBH_4 is used to reduce the diazonium groups of the calixarenes, generating highly reactive radicals that can react with the silver surface.⁴¹ Calix[4]arene-modified AgNPs were characterized by dynamic light scattering (DLS), UV-Vis and ATR-FTIR spectroscopies as well as scanning and transmission electronic microscopy (SEM and TEM). **Figure 2A** shows that all the $\text{AgNPs}^{\text{Df-C1}}$ suspensions possessed a sharp and intense LSPR band that is the signature of well-dispersed nanomaterials. Interestingly, if compared to $\text{AgNPs}^{\text{Df-citrate}}$, the functionalization with **C1** induced a red shift of the AgNPs LSPR band for Df up to 8 but, for the batches obtained with the largest Df , a blue shift was observed. **Figure 2B** shows the corresponding pictures of the $\text{AgNPs}^{\text{Df-C1}}$ suspensions. For Df of 40 or higher, the position of the maximum of absorption was out of the visible region and the color of the sample became pale grey. DLS analysis of $\text{AgNPs}^{\text{Df-C1}}$ suspensions showed that the size of the particles is proportional to the dilution factor of the initial seeds AgNPs^0 (**Figure 2C**). Similar results were obtained with $\text{AgNPs}^{\text{Df-C2}}$ suspensions (see Figure S1).

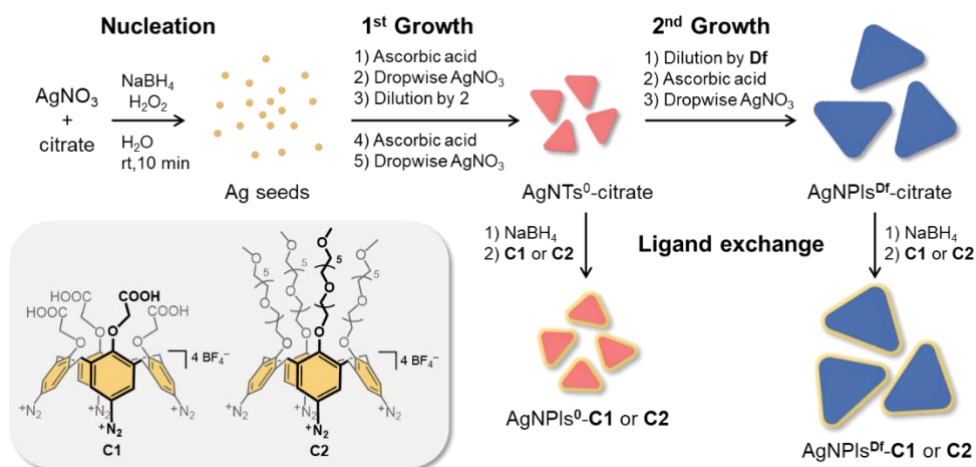


Figure 1. Synthesis of calixarene-coated $\text{AgNPs}^0\text{-C1}$, $\text{AgNPs}^0\text{-C2}$, $\text{AgNPs}^{\text{Df-C1}}$ or $\text{AgNPs}^{\text{Df-C2}}$. Df = dilution factor. Inset: structure of the calixarene-tetradiazonium salts **C1** and **C2**.

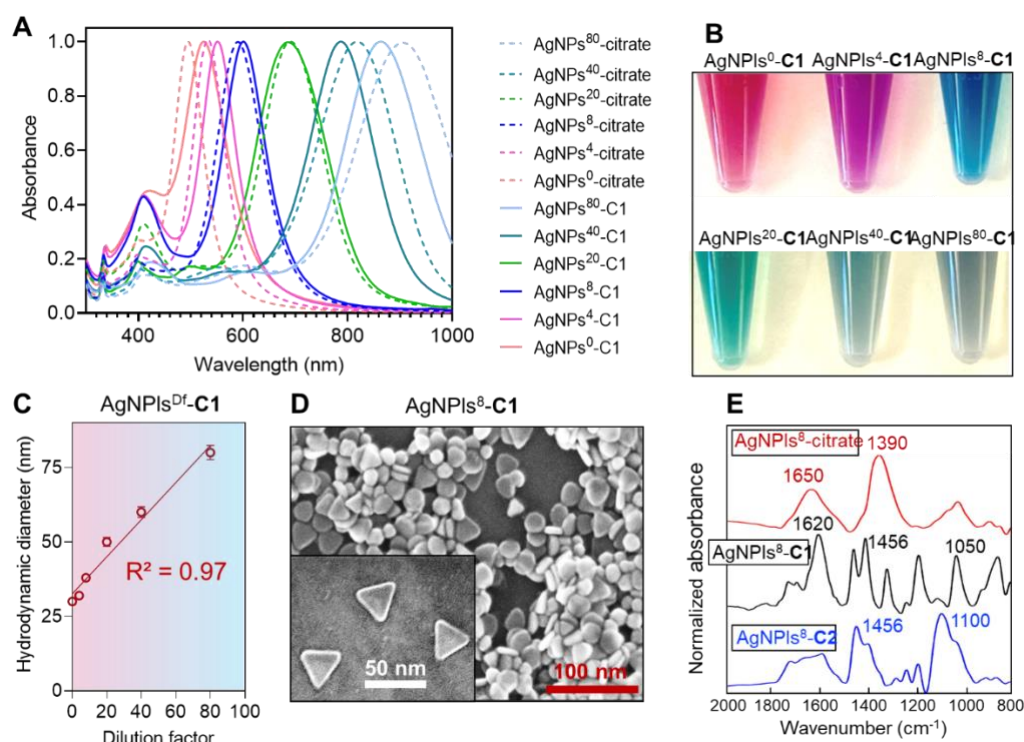


Figure 2. Characterization of AgNPs^{Df}-C1. (A) Normalized UV-Vis spectra of AgNPs⁰-citrate and AgNPs^{Df}-citrate (dashed lines) and the corresponding AgNPs⁰-C1 of AgNPs^{Df}-C1 suspended in pure water (plain lines). (B) Pictures of AgNPs⁰-C1 and AgNPs^{Df}-C1. (C) Hydrodynamic diameter of AgNPs⁰-C1 and AgNPs^{Df}-C1 (determined through DLS analyses) as function of the dilution factor. (D) SEM image of AgNPs⁸-C1. (E) ATR-FTIR spectra of AgNPs⁸-citrate (red), AgNPs⁸-C1 (black) or AgNPs⁸-C2 (blue).

SEM and TEM analyses of the dried suspensions revealed triangular shapes despite the strong etching of the edge of the plates upon exposure to the electron beam. **Figure 2D** shows SEM pictures of AgNPs⁸-C1 and core sizes of approximately 30 nm were measured (see supporting information Figure S1D for SEM and TEM images of AgNPs²⁰-C2 and Figure S2 for TEM images AgNPs⁸⁰-C1). Interestingly, DLS measurement for AgNPs⁸-C1 revealed a hydrodynamic diameter of 38 nm which, considering the average size measured by TEM, corresponds to a thin calixarene layer around the AgNPs. Finally, the grafting of the calixarenes was confirmed with ATR-FTIR spectroscopy, as signature of **C1** (i.e. C_{ar}-C_{ar} at 1456 cm⁻¹ and C=O at 1620 cm⁻¹ and 1050 cm⁻¹) and **C2** (i.e. C_{ar}-C_{ar} at 1456 cm⁻¹ and COC at 1100 cm⁻¹) were observed on AgNPs-C1 and AgNPs-C2, respectively. **Figure 2E** shows, as an example, the ATR-FTIR spectra of AgNPs⁸-C1 and AgNPs⁸-C2. It is worth noting that no more signals corresponding to citrate anions (typically at 1650

and 1390 cm⁻¹) could be observed, clearly indicating that the ligand exchange process was efficient. For comparison purpose, ATR-FTIR spectra of the calixarenes **C1** and **C2** as well as AgNPs⁸-citrate can be found in the Supporting Information (Figure S3).

Stability of AgNPs^{Df}-C1 and AgNPs^{Df}-C2. The colloidal and chemical stabilities of AgNPs^{Df}-C1 and AgNPs^{Df}-C2 were evaluated by UV-Vis spectroscopy and compared to those of AgNPs⁰-citrate. As similar results were obtained for NTs of all the sizes, for the sake of conciseness, only the stability studies achieved with suspensions of AgNPs⁸ are described here (see Figures S4-S7 for the other sizes of AgNPs). When stored in water at room temperature in a closed vial (glass or plastic) in the dark and without any precaution from air, strong degradation of AgNPs⁸-citrate occurred only one day after their synthesis, as shown by the significant blue-shift of ca. 200 nm of their LSPR band maximum (**Figure 3A**). In contrast, under the same storage conditions, no variation of the LSPR band of

AgNPs⁸-C1 and AgNPs⁸-C2 was observed after one day and only minor changes were apparent over an extremely long period of 900 days (Figures 3B and 3C). Even more remarkably, no loss of particles was observed upon the drying of AgNPs⁸-C2 and their resuspension in pure water two weeks later (Figure 3D). This remarkable result shows that the surface protection conferred by calixarenes allows a long-term storage of AgNPs, even as a powder. It enables an easy handling, storage and transport of these nanomaterials, and paves the way to their widespread use in sensing applications. Moreover, the calixarene-coated AgNPs didn't show any sign of degradation while suspended in 33% saline phosphate buffer (PBS) or in acidic conditions for 2 hours (Figures 3F and 3G). The stability in PBS is crucial for the conjugation of various biomolecules, such as antibodies, to these particles. It is worth noting that the decrease in intensity of the LSPR band of AgNPs⁸-C2 in PBS was due to the sticking of the AgNPs onto the wall of the cuvette and not to a partial degradation of the particles (Figure S8). For comparison, AgNPs⁸-citrate degraded immediately when exposed to similar conditions (Figure 3E): acidic conditions led to the spherization

of these particles, while dispersion in PBS induced their total dissolution as evidenced by the color change of the suspensions that turned from blue to yellow or clear, respectively. It is worth to mention that both AgNPs⁸-C1 and AgNPs⁸-C2 were stable in alkaline conditions and could even endure cycle of pH variation from 7 to 5 then 11 (Figure S9).

Finally, the stability of the calixarene-coated AgNPs in pure pooled human plasma was evaluated by UV-Vis spectroscopy. For this, AgNPs⁴⁰ were chosen because of the position of their maximum of absorption that was out of the absorption of human serum (300-600 nm). No degradation or shape modification of AgNPs⁴⁰-C1 or AgNPs⁴⁰-C2 was detected after 3 hours of incubation in plasma (Figure 3H). It is noteworthy that a red shift of the LSPR band, due to the probable formation of a protein corona, was observed in the case of AgNPs⁴⁰-C1. Interestingly, the different behavior in the case of AgNPs⁴⁰-C2 may be explained by the presence of the PEG layer that prevents the non-specific adsorption of proteins on their surface.⁴²

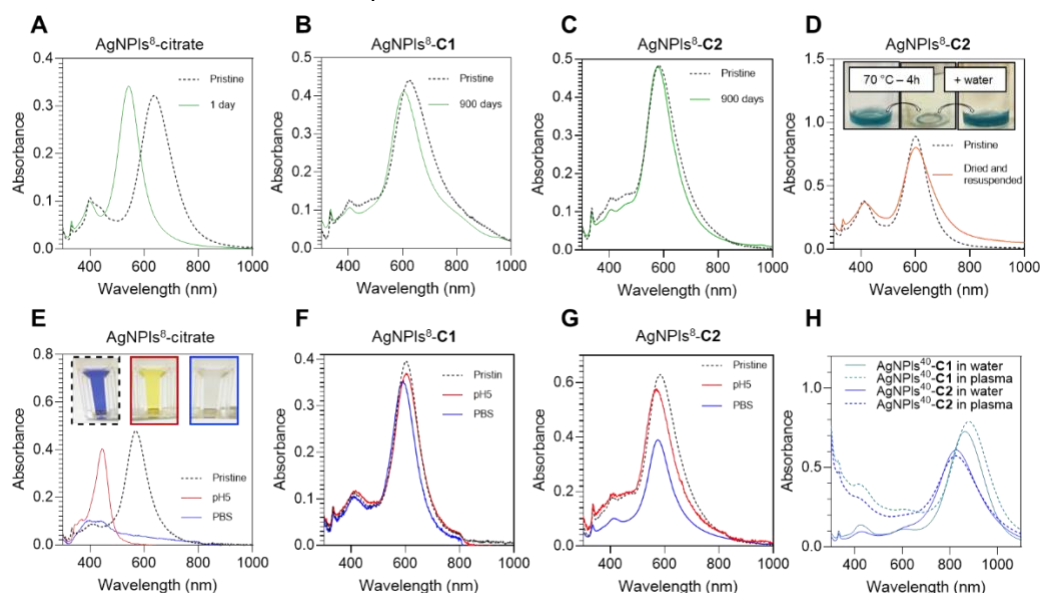


Figure 3. Comparative stability study of AgNPs⁸-citrate, AgNPs⁸-C1 and AgNPs⁸-C2. UV-Vis spectra of (A) AgNPs⁸-citrate right after the synthesis (pristine) or after one day of storage in pure water. UV-Vis spectra of (B) AgNPs⁸-C1 and (C) AgNPs⁸-C2 right after the synthesis (pristine) or after 900 days of storage in pure water. (D) UV-Vis spectra of AgNPs⁸-C2 before and after drying and resuspension in pure water. Insets show the pictures of the corresponding samples. UV-Vis spectra of (E) AgNPs⁸-citrate, (F) AgNPs⁸-C1 or (G) AgNPs⁸-C2 after 2 hours of suspension either in water, acidic condition (pH=5) or 33%

PBS. Insets show pictures or the suspensions. **(H)** UV-Vis spectra of AgNPs⁴⁰-**C1** and AgNPs⁴⁰-**C2**, 3 hours after suspension in either water or pooled human plasma.

These results demonstrate that the calixarene-based coating confers to the silver nanoplates a unique combination of colloidal and chemical stabilities that make them suitable for the development of colorimetric detection tests and more particularly, of serological dipstick assays.

Use of calixarene-coated AgNPs in dipstick assays.

As a proof of concept, AgNPs^{Df}-**C1** were evaluated as colorimetric reporters in a dipstick assay for the detection of Rabbit immunoglobulin G (Rabbit IgG). The dipstick consisted in a nitrocellulose membrane functionalized with an Anti-Rabbit IgG test line (T) and an absorbent pad (**Figure 4A**). First, Anti-Rabbit-IgG was conjugated to AgNPs^{Df}-**C1** (with Df = 4, 8, 20, 40 and 80) through the formation of amide bonds between the carboxyl groups of **C1** and the primary amine groups of the IgG under classical EDC/sulfo-NHS conditions. Thanks to the ultrastability conferred by the calixarene coating,

AgNPs^{Df}-**C1** were able to endure the bioconjugation conditions (i.e. dispersion in MES, centrifugation and redispersion in PBS buffer) and the resulting AgNPs^{Df}-**C1**-Anti-Rabbit-IgG could even be purified from excess of reagents and unbound Anti-Rabbit-IgG via multiple centrifugation cycles. In strong contrast, AgNPs^{Df}-citrate could not be even dispersed in the conjugation buffer without degradation of the particles. As a representative example, **Figure 4B** shows the LSPR band of AgNPs⁸-**C1** before and after conjugation with Anti-Rabbit IgG (see Figure S10 for the UV-Vis of the other AgNPs⁸-**C1**-Anti-Rabbit-IgG). A shift of approximately 5% of the maximum of absorption was observed (i.e. 40 nm for AgNPs⁸-**C1**), confirming the immobilization of the antibodies. All the experimental details regarding the preparation of the dipsticks with the various AgNPs^{Df} can be found in the experimental section.

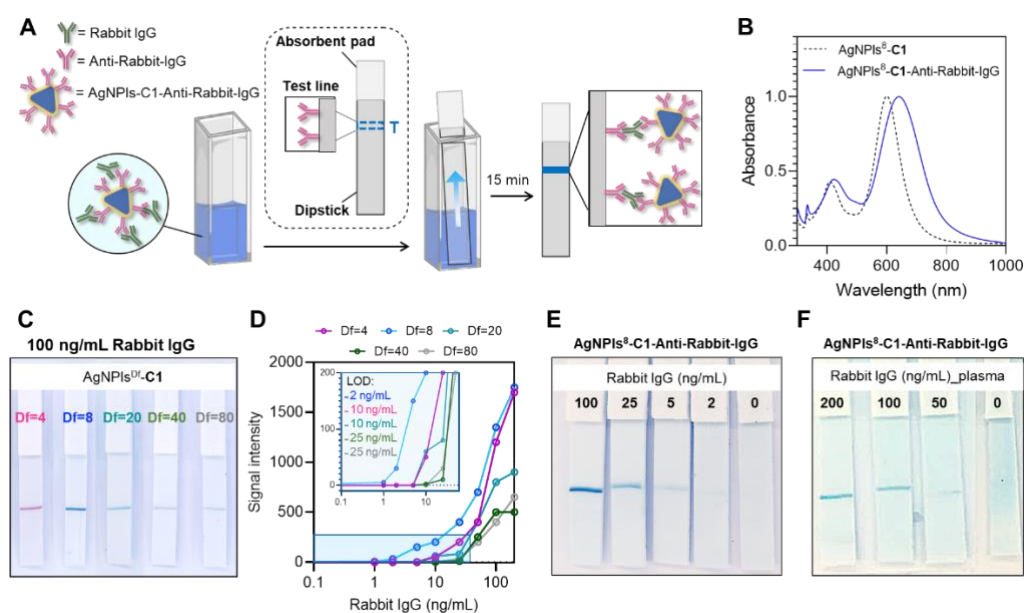


Figure 4. Use of calixarene-coated AgNPs in dipstick assays. (A) Principle of dipstick assays with antibodies-modified AgNPs^{Df}-**C1**. **(B)** UV-Vis spectra of AgNPs⁸-**C1** before and after bioconjugation to Anti-Rabbit-IgG antibodies via EDC/NHS chemistry. **(C)** Pictures of the dipstick assays for the detection of 100 ng/mL of Rabbit IgG spiked in buffer with the different AgNPs^{Df}-**C1**-Anti-Rabbit-IgG reporters. **(D)** Signal intensity as a function of the concentration of Rabbit IgG spiked in buffer for the detection with AgNPs^{Df}-**C1**-Anti-Rabbit-IgG. Inset shows an enlargement of the low IgG concentration region and the estimated LOD for the different sets of NTs. **(E)** Pictures of the dipstick assays for the detection of various concentrations of Rabbit IgG with AgNPs⁸-**C1**-Anti-Rabbit-IgG. **(F)** Pictures of the dipstick assay for the detection of various concentration of Rabbit IgG spiked in human plasma with AgNPs⁸-**C1**-Anti-Rabbit-IgG.

The AgNPLs^{Df}-C1-Anti-Rabbit-IgG were mixed with the samples containing the Rabbit IgG for 15 minutes and then the dipstick was immersed in the solution (**Figure 4A**). The liquid migrated entirely towards the absorbent pad in 15 minutes. To our delight, an unambiguous colored band was observed on all dipsticks, showing that Rabbit IgG could be detected with all the samples of AgNPLs^{Df}-C1-Anti-Rabbit-IgG and confirming the success of the bioconjugation (**Figure 4C**). The detection of 100 ng/mL of Rabbit IgG was evaluated with all the AgNPLs^{Df}-C1-Anti-Rabbit-IgG (D_f ranging from 4 to 80). It is worth noting that AgNPLs^{Df}-C1-Anti-Rabbit-IgG produced with a D_f of 4 or 8 gave the most easily detectable signal to the naked eye, as they strongly absorb visible light. The detection of various concentrations of Rabbit IgG was then studied and the software GelAnalyzer was used to quantitatively assess the limit of detection (LOD).⁴³

The best LOD (2 ng/mL or 10 pM) was found for AgNPLs⁸-C1 (**Figure 4D**). The LOD with the naked eye was slightly higher (5 ng/mL or 25 pM) (**Figure 4E**). Pictures of all the dipstick assays are available in the Supporting Information (Figure S11). Finally, the detection of various concentration of Rabbit IgG was evaluated in spiked pooled human plasma with AgNPLs⁸-C1-Anti-Rabbit-IgG (**Figure 4F**). Firstly, no false positive was observed in the absence of Rabbit IgG, indicating that no non-specific interaction

occurred between the AgNPLs and the Anti-Rabbit-IgGs deposited on the membrane. Importantly, similar results were observed for other AgNPLs^{Df}-C1-Anti-Rabbit-IgG (Figure S12). While the visual LOD was higher than the one in buffer (50 ng/mL vs 5 ng/mL), it still corresponds to the detection of a concentration of 250 pM of Rabbit IgG, which competes with traditional enzyme-linked immunosorbent assay (ELISA). However, dipstick assays offer a more convenient, cost-effective and fast detection procedure that enables a point-of-care testing.

Serological detection of Anti-SARS-CoV-2 IgG with AgNPLs⁸-C1. We next investigated the possibility to detect Anti-SARS-CoV-2 IgG through a sandwich dipstick test using AgNPLs⁸-C1 as the colorimetric reporter. The Receptor-Binding Domain (RBD) of SARS-CoV-2 spike protein was used for the recognition Anti-SARS-CoV-2 immunoglobulins G (see Figure S13 for the protein model).⁴⁴ The RBD was conjugated to AgNPLs⁸-C1 through a classical EDC/sulfo-NHS procedure (see above) and the test line of the dipstick membrane was modified with Anti-Human IgG. In the presence of Anti-SARS-CoV-2 IgGs, AgNPLs will be immobilized at the level of the test line by the formation of a ternary complex Anti-Human IgG_Anti-SARS-CoV-2 IgG_AgNPLs⁸-C1-RBD (**Figure 5A**).

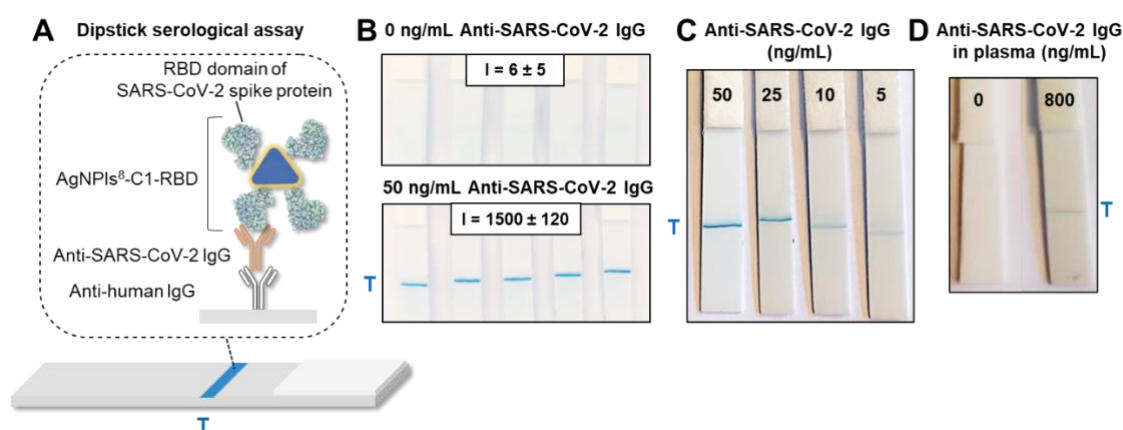


Figure 5. Dipstick serological assay for the detection of Anti-SARS-CoV-2 IgG. (A) Principle of the detection through the formation of a ternary complex. (B) Pictures of five replicates of the dipstick assay for either 0 (top) or 50 ng/mL (bottom) of Anti-SARS-CoV-2 IgG spiked in PBS. Insets report the average intensity (I) quantified using GelAnalyzer. (C) Pictures of the

dipstick assays for different concentrations of Anti-SARS-CoV-2 IgG spiked in PBS used to determine the limit of detection. **(D)** Detection of 800 ng/mL (5 nM) of Anti-SARS-CoV-2 IgG spiked in pure pooled human plasma.

Five replicates of tests were performed in PBS buffer spiked with either 0 or 50 ng/mL of Anti-SARS-CoV-2 IgG (**Figure 5B**). No false positive was observed, and Anti-SARS-CoV-2 IgG could be detected in buffer with a high reproducibility. Moreover, the quantification of the band intensities (I) with GelAnalyzer revealed a standard deviation lower than 10%, which is considered viable for such a system.⁴⁵ A visual LOD of 5 ng/mL was then determined by five operators, which is similar to what we have obtained with Rabbit IgG, indicating that our system is adaptable to different targets without any loss of sensitivity (**Figure 5C**). In pooled human plasma, a LOD of 800 ng/mL was obtained (**Figure 5D**), which is explained by the numerous immunoglobulins present in the plasma that can bind to the Anti-Human IgG on the strip membrane. However, 800 ng/mL represents a concentration of 5 nM, which is respectively two and twenty times better than what we have recently reported with a similar system using spherical 20 nm AgNPs and AuNPs,²² as postulated from their higher extinction coefficient than classical isotropic nanospheres.

Finally, we have investigated the possibility to develop multicolor multiplex assays by exploiting the wide range of colors accessible with the different nanostructures at our disposal. It is worth mentioning that using AgNPs of different sizes, and therefore colors, would allow an easy detection of cross-reactivity between the different target proteins and the antibodies deposited on the different test lines or on the colorimetric reporters. As a proof of concept, we designed a dipstick test for the simultaneous detection of Anti-SARS-CoV-2 (test line T1) IgG and Rabbit IgG (test line T2) with AgNPs⁸-C1-RBD (blue) and AgNPs⁴-C1-Anti-Rabbit-IgG (magenta) (**Figure 6A**). AgNPs⁴-C1-Anti-Rabbit-IgG and AgNPs⁸-C1-RBD were mixed with samples containing either 50 ng/mL of Rabbit IgG, 50 ng/mL of Anti-SARS-CoV-2 IgG, both or none. No band was observed in the absence of both targets while two bands, one magenta and one blue, were observed in their presence (**Figure 6B**). Importantly, no cross-reactivity was observed as only one magenta band was observed for sample containing only Rabbit IgG and one blue band for sample containing only Anti-SARS-CoV-2 IgG.

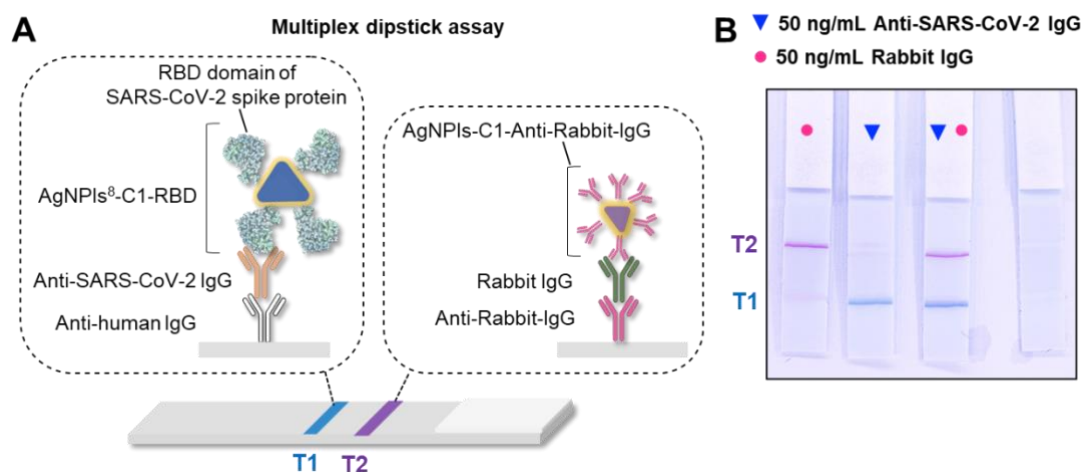


Figure 6. Multiplex dipstick assay for the simultaneous detection of Anti-SARS-CoV-2 IgG and Rabbit IgG. (A) Principle of the detection through the formation of ternary complexes. Anti-Human IgG and Anti-Rabbit IgG were respectively deposited on tests lines T1 and T2 on the dipstick. The running buffer contains both AgNPs⁸-C1-RBD and AgNPs⁴-C1-Anti-Rabbit-IgG and the samples either Anti-SARS-CoV-2 IgG, Rabbit IgG or both. **(B)** Pictures of the multiplex dipstick assays obtained with samples containing either 50 ng/mL of Rabbit IgG, Anti-SARS-CoV-2 IgG, both spiked in PBS or none.

These findings clearly demonstrate the remarkable potential of AgNPLs for the design multiplex dipstick assays and pave the way to the use of these nanomaterials in biosensing applications.

Experimental

AgNPLs⁰ synthesis. Unless specified, all the solutions were aqueous. In a 30 mL glass vial, 21.1±0.3 mg of trisodium citrate are dissolved in 19.65 mL of MilliQ water under magnetic stirring. To this, 93 µL of AgNO₃ (10 mM), 12.8 µL of H₂O₂ (6% vol./vol.) and 96 µL of NaBH₄ (100 mM) were added and the resulting solution was vigorously stirred for 9 minutes. The solution turned from clear to pale yellow. Then, 200 µL of L-Ascorbic acid (50 mM) were added, followed by a drop-wise addition of 500 µL of AgNO₃ (10 mM). Typically, 10 additions of 50 µL were performed at 50 seconds time intervals. The solution turned from yellow to red. Next, the solution was diluted two times (10 mL + 10 mL of MilliQ water) and 100 µL of L-Ascorbic acid (50 mM) were added, followed by a drop-wise addition of 250 µL (5x50 µL) of AgNO₃ (10 mM). The solution turned pink and the resulting AgNPLs were named AgNPLs⁰. AgNPLs⁰ were then used as precursor to produce larger AgNPLs.

Synthesis of AgNPLs^{Df}. Larger AgNPLs were synthesized from dilution of AgNPLs⁰ in MilliQ water. The dilution factor (D_f) dictates the final size of the AgNPLs, labelled AgNPLs⁰. We describe here the example of AgNPLs⁸: 2.5 mL of AgNPLs⁰ were mixed with 17.5 mL of MilliQ water and then 100 µL of L-Ascorbic Acid (50 mM) were added under stirring and 200 µL of AgNO₃ (10 mM) were added dropwise (10 x 20 µL) with a waiting time of 30 sec between two additions.

Coating of AgNPLs^{Df} with C1 and C2. In a 4 mL glass vial, 3.8 mL of AgNPLs^{Df} were mixed with 40 µL NaBH₄ (100 mM) and then 200 µL of C1 or C2 (5 mM) were added dropwise at 2 sec time intervals and the resulting solution was stirred overnight at room temperature. The AgNPLs^{Df}-C1 or -C2 were then cleaned of excess reagents by centrifugation

at 15.000g for 20 minutes. Typically, 8 µL of NaOH 1M were added to the crude solution and then two centrifugation cycles were performed with removal of the supernatant and replacement by an equivalent volume of a 5mM NaOH solution after the first centrifugation and MilliQ water for the second one. The cleaned nanoplates were stored at room temperature in the dark.

Conjugation of biomolecules to AgNPLs^{Df}-C1. First, the activation of the carboxyl groups of AgNPLs^{Df}-C1 was conducted as follows: 500 µL AgNPLs^{Df}-C1 (OD=4) were mixed to 50 µL of MES buffer (100 mM, pH 5.8), 10 µL of EDC.HCl (6 mM) and 10 µL of sulfo-NHS (10 mM) in a 1.5 mL Protein Lobind Eppendorf. The activation step lasted 30 minutes, after which, the activated AgNPLs^{Df}-C1 were centrifuged (15.000g/15 minutes) and the supernatant was replaced by MilliQ water. Then, 8 µL Anti-Rabbit IgG (2 mg/mL) or 3 µL of Prot-S (30 µM) were added and the reaction was stirred 4 hours at 1000 rpm and room temperature. After the incubation, the conjugated particles were cleaned from excess of biomolecules with two cycles of centrifugation (15.000/15minutes) and replacement of the supernatant by MilliQ water.

Assembly of the dipstick assay. Anti-Rabbit IgG (2 mg/mL) or Goat Anti-Human IgG (2 mg/mL) were dispensed on the nitrocellulose membrane to prepare the dipstick assays for Rabbit IgG or Anti-SARS-CoV-2 IgG detection respectively. Nitrocellulose membranes were incubated at 37 °C for 2 hours to allow the antibodies solutions to dry. Finally, the absorbent pad was stuck on the top of the nitrocellulose.

Dipstick Assay. In a disposable cuvette, 5 µL of AgNPLs^{Df}-C1-Anti-Rabbit IgG (OD=3) or 5 µL of AgNPLs^{Df}-C1-RBD were suspended in 40 µL of Abcam running buffer 1x (with 1% BSA) and were mixed for 15 minutes to either Rabbit IgG or Anti-SARS-CoV-2 IgG, respectively. Then, the dipstick was immersed in the solution and this latter migrated entirely toward the absorbent pad in 15 minutes, allowing the visualisation of the colour bands.

Conclusions

Herein we report on a novel surface modification of silver nanoplates with calixarene-diazonium salts and their use as colorimetric reporters in dipstick assays. Our synthesis procedure allowed to produce calixarene-coated nanoplates with a core size depending only on the dilution factor of a precursor solution in the growth solution. We demonstrated the coating of AgNPLs with two calixarenes differing by their substituents at the level of their small rim, one bearing four carboxylate groups, **C1**, the other four PEG chains, **C2**. These calixarenes were selected as they confer distinct properties to the surfaces on which they are grafted: **C1** ensure the colloidal stability of particles at pH > 6 and can serve to the covalent conjugation of biomolecules through the formation of amide bonds while **C2** leads to a dense PEG layer that enables a steric stabilization of the particles.¹⁹ After characterization of the calixarene coating, the improvement of the colloidal and chemical stabilities of the calixarene-coated AgNPLs was assessed. The calixarene-coating increased drastically the lifetime of the nanoplates and allowed their dispersion in PBS, acidic conditions as well as in biofluids without any loss of stability or degradation, in contrast to AgNPLs-citrate that degrade totally in all tested conditions. Due to their high stability, calixarene-coated AgNPLs could be conjugated with antibodies via EDC/NHS cross-linking and consequently exploited in dipstick assays. The detection of Rabbit IgG was first demonstrated as proof-of-concept and picomolar limit of detection in plasma was obtained, which compete with ELISA sensitivity. Finally, the system was extended to the detection of Anti-SARS-CoV-2 IgG and a limit of detection of 5 nM was obtain in pure human plasma. This LOD is two times better than the one previously obtained with 20-nm silver spherical particles, and twenty times better than the one reported with similar AuNPs. Importantly, it was possible to use calixarene-coated AgNPLs of different sizes for the simultaneous detection of multiple analytes such as Rabbit IgG and Anti-SARS-CoV-2 IgG. Our findings are of broad interest for anyone designing serological dipstick or lateral-flow

assays as calixarene-coated AgNPLs can improve the sensitivity of nanomaterial-based systems while reducing the number of particles per tests and allow to tune the color of the detection band. In addition, having nanoparticles of different nature, size and shape, displaying light extinction properties that can vary by several orders of magnitude, opens the way to the detection of analytes whose respective concentrations can vary by several orders of magnitude or to probe a single analyte over an extended dynamic range. Also, the design of multicolor multiplex assays is particularly adapted to serological testing with the simultaneous detection of different immunoglobulins (A, G, M).

Conflicts of interest

M. R. was a postdoctoral researcher for X4C from August 2020 to January 2021. I. J. is a shareholder of X4C. I. J. and G.B. are consultants for X4C.

Acknowledgements

The Fonds pour la formation à la Recherche dans l'Industrie et dans l'Agriculture (FRIA-FRS, Belgium, PhD grant to B. G.), the "Actions de Recherches Concertées" of the Fédération Wallonie-Bruxelles and the ULB (PhD grant to M. R. and P. B.) are acknowledged for financial support. G. B. and I. J. thank the "fonds Jaumotte-Demoulin" for funding.

Notes and references

- [1] S. Mitragotri, D. G. Anderson, X. Chen, E. K. Chow, D. Ho, A. V. Kabanov, J. M. Karp, K. Kataoka, C. A. Mirkin, S. H. Petrosko, J. Shi, O. M. M. Stevens, S. Sun, S. Teoh, S. S. Venkatraman, Y. Xia, S. Wang, Z. Gu, C. Xu, *ACS Nano*, 2015, **9**, 6644–6654.
- [2] A. Umapathi, M. Kumawat, H. K. Daima, *Environ. Chem. Lett.*, 2022, **20**, 445–468.
- [3] E. Hutter, J. H. H. Fendler, *Advanced Materials*, 2004, **16**, 1685–1706.
- [4] N. G. Khlebtsov, L. A. Dykman, *J. Quant. Spectrosc. Radiat. Transf.*, 2010, **111**, 1–35.
- [5] D. D. Gurav, Y. Jia, J. Ye, K. Qian, *Nanoscale adv.*, 2019, **1**, 459–469.
- [6] M. Falahati, F. Attar, M. Sharifi, A. A. Saboury, A. Salihi, F. M. Aziz, I. Kostova, C. Burda, P. Prielcel, J. A. Lopez-Sanchez, S. Laurent, N. Hooshmand, M. A. El-Sayed, *Biochim. Biophys. Acta. Gen. Subj.*, 2020, **1864**, 129435
- [7] J. Kimling, M. Maier, B. Okenve, V. Kotaidis, H. Ballot, A. Plech, *J. Phys. Chem. B*, 2006, **110**, 15700–15707.
- [8] N. Elahi, M. Kamali, M. H. Baghersad, *Talanta*, 2018, **184**, 537–556.
- [9] M. Sharifi, F. Attar, A. A. Saboury, K. Akhtari, N. Hooshmand, A. Hasan, M. A. El-Sayed, M. Falahati, *J. Control. Release*, 2019, **311**, 170–189.
- [10] J. Sun, Y. Lu, L. He, J. Pang, F. Yang, Y. Liu, *TrAC - Trends Anal. Chem.*, 2020, **122**, 115754.

- [11] M. S. Draz, H. Shafiee, *Theranostics*, 2018, **8**, 1985–2017.
- [12] M. Retout, H. Valkenier, E. Triffaux, T. Doneux, K. Bartik, G. Bruylants, *ACS Sensors*, 2016, **1**, 929–933.
- [13] Z. Jin, Y. Mantri, M. Retout, Y. Cheng, J. Zhou, A. Jorns, P. Fajtova, W. Yim, C. Moore, M. Xu, M. Creyer, R. Borum, J. Zhou, Z. Wu, T. He, W. Penny, A. O'Donoghue, J. Jokerst, *Angew. Chem. Int. Edit.*, 2022, **61**, e202112995
- [14] F. Xia, X. Zuo, R. Yang, Y. Xiao, D. Kang, A. Vallée-Bélisle, X. Gong, J. D. Yuen, B. B. Y. Hsu, A. J. Heeger, K. W. Plaxco, *Proc. Natl. Acad. Sci. U S A*, 2010, **107**, 10837–10841.
- [15] D. Paramelle, A. Sadvoy, S. Gorelik, P. Free, J. Hobley, D. G. Fernig, *Analyst*, 2014, **139**, 4855–4861.
- [16] Y. Han, R. Lupitsky, T. M. Chou, C. M. Stafford, H. Du, S. Sukhishvili, *Anal. Chem.*, 2011, **83**, 5873–5880.
- [17] I. Pinzaru, D. Coricovac, C. Dehelean, E. A. Moacă, M. Mioc, F. Baderca, I. Sizemore, S. Brittle, D. Marti, C. D. Calina, A. M. Tsatsakis, C. Şoica, *Food Chem. Toxicol.*, 2018, **111**, 546–556.
- [18] M. Sabela, S. Balme, M. Bechelany, J. M. Janot, K. Bisetty, *Adv. Eng. Mater.*, 2017, **19**, 1–24.
- [19] M. Retout, I. Jabin, G. Bruylants, *ACS Omega*, 2021, **6**, 19675–19684.
- [20] Q. Lenne, M. Retout, B. Gosselin, G. Bruylants, I. Jabin, J. Hamon, C. Lagrost, Y. R. Leroux, *Chem. Commun.*, 2022, **58**, 3334–3337.
- [21] M. Retout, B. Gosselin, A. Mattiuzzi, I. Ternad, I. Jabin, G. Bruylants, *Chempluschem*, 2022, **87**, e202100450.
- [22] B. Gosselin, M. Retout, L. Troian-gautier, R. Bevernaegie, O. Denis, G. Bruylants, I. Jabin, S. Herens, P. Lefe, *Anal. Chem.*, 2022, **94**, 7383–7390.
- [23] L. Troian-Gautier, A. Mattiuzzi, O. Reinaud, C. Lagrost, I. Jabin, *Org. Biomol. Chem.*, 2020, **18**, 3624–3637.
- [24] A. Mattiuzzi, I. Jabin, C. Mangeney, C. Roux, O. Reinaud, L. Santos, J. F. Bergamini, P. Hapiot, C. Lagrost, *Nat. Commun.*, 2012, **3**, 1130.
- [25] H. Valkenier, V. Malytskyi, P. Blond, M. Retout, A. Mattiuzzi, J. Goole, V. Raussens, I. Jabin, G. Bruylants, *Langmuir*, 2017, **33**, 8253–8259.
- [26] M. Retout, P. Blond, I. Jabin, G. Bruylants, *Bioconjugate Chem.*, 2021, **32**, 290–300.
- [27] M. Retout, B. Cornelio, G. Bruylants, I. Jabin, *Langmuir*, 2022, **38**, 9301–9309.
- [28] Y. Yang, J. Murray, J. Haverstick, R. A. Tripp, Y. Zhao, *Sens. Actuators B Chem.*, 2022, **359**, 131604.
- [29] M. Retout, Y. Mantri, Z. Jin, J. Zhou, G. Noël, B. Donovan, W. Yim, J. v. Jokerst, *ACS Nano*, 2022, **16**, 6165–6175.
- [30] M. N. Creyer, Z. Jin, C. Moore, W. Yim, J. Zhou, J. v. Jokerst, *ACS Appl. Mater. Interfaces*, 2021, **13**, 45236–45243.
- [31] M. N. Creyer, Z. Jin, M. Retout, W. Yim, J. Zhou, J. v. Jokerst, *Langmuir*, 2022, **38**, 14200–14207.
- [32] Y. Sun, G. P. Wiederrecht, *Small*, 2007, **3**, 1964–1975.
- [33] J. Haber, K. Sokolov, *Langmuir*, 2017, **33**, 10525–10530.
- [34] B. Tang, S. Xu, X. Hou, J. Li, L. Sun, W. Xu, X. Wang, *ACS Appl. Mater. Interfaces*, 2013, **5**, 646–653.
- [35] Q. Zhang, J. Ge, T. Pham, J. Goebel, Y. Hu, Z. Lu, Y. Yin, *Angew. Chem. Int. Ed.*, 2009, **48**, 3516–3519.
- [36] M. Kim, Y. W. Lee, D. Kim, S. Lee, S. R. Ryoo, D. H. Min, S. B. Lee, S. W. Han, *ACS Appl. Mater. Interfaces*, 2012, **4**, 5038–5043.
- [37] K. A. Homan, M. Souza, R. Truby, G. P. Luke, C. Green, E. Vreeland, S. Emelianov, *ACS Nano*, 2012, **6**, 641–650.
- [38] X. Le Guével, F. Y. Wang, O. Stranik, R. Nooney, V. Gubala, C. McDonagh, B. D. MacCraith, *J. Phys. Chem. C*, 2009, **113**, 16380–16386.
- [39] C. W. Yen, H. de Puig, J. O. Tam, J. Gómez-Márquez, I. Bosch, K. Hamad-Schifferli, L. Gehrke, *Lab Chip*, 2015, **15**, 1638–1641.
- [40] S. Vinayagam, P. Rajaiah, A. Mukherjee, C. Natarajan, *Spectrochim. Acta A Mol. Biomol. Spectrosc.*, 2018, **202**, 346–351.
- [41] J. Pinson, F. Podvoricab, *Chem. Soc. Rev.*, 2005, **34**, 429–439.
- [42] P. Blond, R. Bevernaegie, L. Troian-Gautier, C. Lagrost, J. Hubert, F. Reniers, V. Raussens, I. Jabin, *Langmuir*, 2020, **36**, 12068–12076.
- [43] GelAnalyzer 19.1 (www.gelanalyzer.com) by Istvan Lazar Jr., PhD and Istvan Lazar Sr., PhD, CSC.
- [44] A. Pramanik, Y. Gao, S. Patibandla, D. Mitra, M. G. McCandless, L. A. Fassero, K. Gates, R. Tandon, P. Chandra Ray, *Nanoscale Adv.*, 2021, **3**, 1588–1596.
- [45] L. Anfossi, F. di Nardo, S. Cavalera, C. Giovannoli, C. Baggiani, *Biosensors*, 2018, **9**, 2.